Journal of Inorganic Biochemistry 227 (2022) 111670

Contents lists available at ScienceDirect

Journal of Inorganic Biochemistry

journal homepage: www.elsevier.com/locate/jinorgbio

Neuroprotective effects of fluorophore-labelled manganese complexes: Determination of ROS production, mitochondrial membrane potential and confocal fluorescence microscopy studies in neuroblastoma cells

Lara Rouco [a], Rebeca Alvariño [b,*], Amparo Alfonso [b], María J. Romero [c], Rosa Pedrido [d], Marcelino Maneiro [a,*]

[a] Departamento de Química Inorgánica, Facultade de Ciencias, Campus Terra, Universidade de Santiago de Compostela, Lugo, Spain
[b] Departamento de Farmacología, Facultade de Veterinaria, Campus Terra, Universidade de Santiago de Compostela, Lugo, Spain
[c] Departamento de Didácticas Aplicadas, Facultade de Formación do Profesorado, Campus Terra, Universidade de Santiago de Compostela, Lugo, Spain
[d] Departamento de Química Inorgánica, Facultade de Química, Campus Vida, Universidade de Santiago de Compostela, Santiago de Compostela, Spain

ARTICLE INFO

Keywords:
Manganese
Oxidative stress
Neuroprotection
Schiff bases
Fluorophore
Superoxide dismutase

ABSTRACT

In this work, four manganese(II) complexes derived from the ligands H_2L^1-H_2L^4, that incorporate dansyl or tosyl fluorescent dyes, have been investigated in term of their antioxidant properties. Two of the manganese(II) complexes have been newly prepared using the asymmetric half-salen ligand H_2L^2 and the thiosemicarbazone ligand H_2L^3. The four organic strands and the manganese complexes have been characterized by different analytical and spectroscopic techniques. The study of the antioxidant behaviour of these two new complexes and other two fluorophore-labelled analogues was tested in SH-SY5Y neuroblastoma cells. These four model complexes **1**–**4** were found to protect cells from oxidative damage in this human neuronal model, by reducing the release of reactive oxygen species. Complexes **1**–**4** significantly improved cell survival, with levels between 79.1 ± 0.8% and 130.9 ± 4.1%. Moreover, complexes **3** and **4** were able to restore the mitochondrial membrane potential at 1 μM, with **4** reaching levels higher than 85%, similar to the percentages obtained by the positive control agent cyclosporin A. The incorporation of the fluorescent label in the complexes allowed the study of their ability to enter the human neuroblastoma cells by confocal microscopy.

1. Introduction

Oxidative stress is associated to the development of different pathologies such as inflammatory diseases [1], carcinogenesis [2], type II diabetes [3] or neurodegenerative processes [4–5]. Recent evidence also suggests a correlation between severe COVID-19 symptoms with an increase of oxidative stress as result of the release of cytokines, the so-called cytokine storm syndrome [6–14].

The excess of reactive oxygen species (ROS) is what causes oxidative stress, and there are different endogenous and exogenous sources that can generate this excess [15]. In most situations, living systems can regulate ROS levels through antioxidant defences, among which are antioxidant enzymes such as superoxide dismutase (SOD), catalase (CAT) or glutathione peroxidase (GP) [16]. However, when there is an imbalance between ROS overproduction and the antioxidant system, oxidative stress leads to cell damage and organ failures [17]. Brain is one of the most sensitive organs to oxidative stress due to its high rate of energy consumption and oxygen uptake [18–19]. Recently, we have reported for the first time [20] the neuroprotective effects of Mn(III)-Schiff base complexes in human neuroblastoma SH-SY5Y cells, an in vitro model system for studying oxidative stress [21–22]. The reaction mechanism of these complexes against H_2O_2 appears to be strongly dependent on the conditions.

Synthetic catalytic antioxidants like Mn(III)-Schiff base complexes are low molecular weight SOD/CAT mimics that can facilitate the scavenging of excessive ROS levels and its associated pathologies [23–27], showing beneficial effects in multiple in vitro and in vivo trials [28–31]. For instance, different synthetic models demonstrated efficacy to rescuing rodents from spongiform neurodegenerative disorders [32], ischemia/reperfusion injury [33], Alzheimer's disease [34], age-related cognitive deficits [35], human prion disease [36], ataxia-telangiectasia [37], amyotrophic lateral sclerosis [38], and other neurodegenerative

* Corresponding author.
E-mail addresses: rebeca.alvarino@usc.es (R. Alvariño), marcelino.maneiro@usc.es (M. Maneiro).

https://doi.org/10.1016/j.jinorgbio.2021.111670
Received 2 June 2021; Received in revised form 18 November 2021; Accepted 18 November 2021
Available online 24 November 2021
0162-0134/© 2021 The Author(s). Published by Elsevier Inc. This is an open access article under the CC BY-NC-ND license (http://creativecommons.org/licenses/by-nc-nd/4.0/).

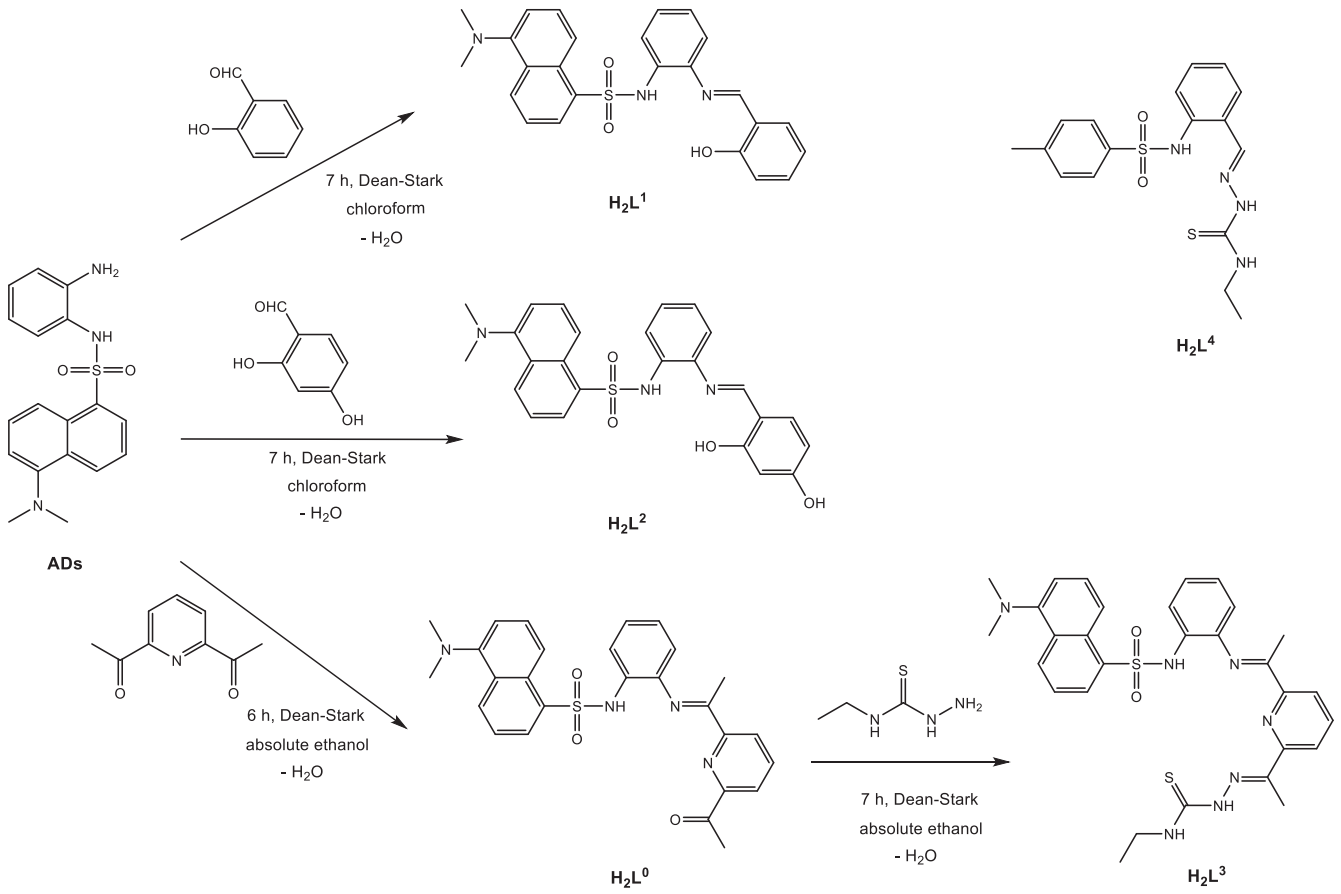

Scheme 1. Structure of the ligands H_2L^1-H_2L^4 and their precursors ADs and H_2L^0.

diseases.

However, much is still unknown about the associated pathophysiological pathways of these synthetic catalytic antioxidants. One of the limitations in knowing how these compounds act is in the availability of techniques that allow monitoring their distribution in cells and tissues, as well as in measuring their evolution during their antioxidant activity in biological media. In this sense, the use of complexes with fluorescent properties in this field thus becomes an avenue to be explored [39].

In the work herein described, we selected four ligands that incorporate a dansyl or a tosyl fluorophore group (see Scheme 1). These fluorophores, characterized by high emission quantum yields, are present in many fluorescent sensors and labels [40–41]. Two of the ligands H_2L^2 and H_2L^3 are newly reported, and, in the case of the latter, it implies the development of a new organic synthesis route. The synthesis of H_2L^1, H_2L^4 and their manganese complexes had been previously reported by us [42–44]. H_2L^1 and H_2L^2 are asymmetric half-salen ligands with a dansyl group and a tridentate [N_2O] donor set which provides a coordination number asymmetry *in tandem*. H_2L^3 and H_2L^4 are organic systems that incorporate thiosemicarbazones and a dansylamide or a tosylamide skeletons, respectively. Then, we examined the cytoprotective effect of four manganese complexes **1**–**4**, obtained from H_2L^1-H_2L^4, against H_2O_2-induced oxidative stress in human neuroblastoma cells. The work includes studies of neuroprotection and mitochondrial membrane potential ($\Delta\Psi_m$) assays, determination of ROS production, and the ability of the complexes to enter SH-SY5Y cells assessed by confocal microscopy.

2. Experimental section

2.1. Materials for synthesis and chemical reactions

All solvents, *o*-phenylenediamine, dansyl chloride, triethylamine, 2,4-dihydroxybenzaldehyde, salicylaldehyde, 2,6-diacetylpyridine, 4-ethyl-3-thiosemicarbazide and tetraethylammonium perchlorate are commercially available and were used without further purification. Manganese metal (Ega Chemie) was used as ca. 2 × 2 cm^2 plate.

The ligands H_2L^1 and H_2L^4 were prepared following the reported procedures [42–44]. H_2L^1, H_2L^2 and H_2L^3 were obtained by condensation of different aldehydes (or a carbonyl precursor in case of H_2L^3) to a solution of the primary amine *N*-(2-aminophenyl)-5-(dimethylamino)-1-naphthalenesulfonamide (ADs). The synthesis of ADs was previously described by us [43]. The synthesis of H_2L^3 involves two steps, with the previous isolation of a carbonyl precursor labelled as H_2L^0. Data for synthesis and characterization of H_2L^0, H_2L^2 and H_2L^3 are available in the supplementary data section.

Complexes **1** ($MnL^1 \cdot 3H_2O$) and **4** ($Mn_2L^4{}_2$) were prepared following the reported procedure [42–44]. Neutral metal complexes **2** and **3** derived from ligands H_2L^2 and H_2L^3 respectively were obtained by an electrochemical methodology.

$MnL^2 \cdot 3H_2O$ (2): A solution of the ligand H_2L^2 (0.1 g, 0.22 mmol) containing tetraethylammonium perchlorate as supporting electrolyte, a platinum wire as cathode and a manganese plate as anode, was electrolysed in degassed acetonitrile (80 mL) for 1 h and 10 min. The reaction was carried out at 10 mA under argon atmosphere. The resulting brownish solution was concentrated under reduced pressure and diethyl ether was added until the precipitation was completed. The brown solid formed was filtered, washed with diethyl ether, and dried in vacuo. Yield 64%. Elemental analysis, Calc. for $MnC_{25}H_{27}N_3O_7S$: C, 52.8; H, 4.8; N, 7.4; S, 5.6. Found: C, 52,5; H, 4.9; N, 7.2; S, 5.8. ESI (*m/z* $[M]^+$): 514.1 $[ML + H]^+$. IR (KBr, cm^{-1}): ν(OH) 3393, ν(C=N + C-N) 1613, 1587, $\nu(SO_2)_{AS}$ 1329, $\nu(SO_2)_S$ 1146. μ_{exp} (B. M.): 5.8. E_{ox} (at 0.02 V s^{-1}) = −0.660 V; E_{red} (at 0.02 V s^{-1}) = −0.790 V; $E_{1/2}$ = −0.73 V;ΔE_p = 130 mV.

$MnL^3 \cdot 4H_2O$ (3): The ligand H_2L^3 (0.1 g, 0.17 mmol) was dissolved

in degassed dry acetonitrile (60 mL) containing tetraethylammonium perchlorate as supporting electrolyte. The solution was electrolysed for 55 min at 10 mA under argon employing a platinum wire as cathode and a manganese plate as anode. After the reaction was finished, the solvent was completely removed by bubbling argon through the orange solution.The solid formed was filtered, washed with dietly ether, and dried in vacuo. Yield 45%. Elemental analysis, Calc. for $MnC_{30}H_{39}N_7O_6S_2$: C, 50.6; H, 5.5; N, 13.8; S, 9.0. Found: C, 50.4; H, 5.4; N, 13.5; S, 8.7. ESI (m/z $[M]^+$): 641.1 $[ML + H]^+$. IR (KBr, cm^{-1}): ν(OH/NH), 3412/ 3213, ν(C=N + C-N) 1630, $\nu(SO_2)_{AS}$ 1325, $\nu(SO_2)_S$ 1148, ν(CS) 1121, 825, ν(N—N) 1049. μ_{exp} (B. M.): 5.9. E_{ox} (at 0.02 V s^{-1}) = −0.730 V; E_{red} (at 0.02 V s^{-1}) = −0.960 V; $E_{1/2}$ = −0.83 V; ΔE_p = 230 mV.

2.2. Cyclic voltammetry measurements

Electrochemical measurements were performed using an Autolab PGSTAT101 using a three-electrode configuration. The working electrode was a Metrohm model 6.1204.300 graphite disc, while a Pt wire and an Ag/AgCl electrode served as counter and reference electrodes, respectively. Measurements were made with ca. 10^{-3} M solutions of complexes in DMSO using 0.1 M tetraethylammonium perchlorate as a supporting electrolyte. The solutions were deoxygenated before each measurement by bubbling N_2. The glassy carbon working electrode was mechanically cleaned before each experiment by polishing its Surface using a polishing kit (Metrohm 6.2802.010), first with α-Al_2O_3 (0.3 μm) and after washed with purified water.

2.3. Cell culture

Human neuroblastoma SH-SY5Y cell line used in this study was purchased from the American Type Culture Collection (ATCC), number CRL2266. Cells were grown in Dulbecco's modified Eagle's medium: Nutrient Mix F-12 (DMEM/F-12) supplemented with 10% fetal bovine serum (FBS), 1% glutamax, 100 U/mL penicillin and 100 μg/mL streptomycin. Cells were incubated in a humidified atmosphere of 5% CO_2 at 37 °C and dissociated weekly using 0.05% trypsin/EDTA. All reagents were provided by Thermo Fisher Scientific (Waltham, MA, USA).

2.4. Cell viability assay

Cells were seeded in 96-well plates at a density of 5×10^4 cells per well, 24 h before treatment. SH-SY5Y cells were treated with manganese complexes **1**–**4** at different concentrations (0.001, 0.01, 0.1, 1 and 10 μM) for 24 h. The effect of compounds on cell viability was evaluated by MTT (3-(4, 5-dimethyl thiazol-2-yl)-2,5-diphenyl tetrazolium bromide) assay [45–46]. SH-SY5Y cells were rinsed three times with Locke's buffer (154 mM NaCl, 5.6 mM KCl, 3.6 mM $NaHCO_3$, 1.3 mM $CaCl_2$, 1 mM $MgCl_2$, 10 mM Hepes, and 5 mM glucose, pH 7.4) and 200 μL of MTT (500 μg/mL; Merck, Darmstadt, Germany) dissolved in saline buffer were added to each well. Following 1 h of incubation at 37 °C, SH-SY5Y cells were disaggregated with 5% sodium dodecyl sulphate. Absorbance of formazan crystals was measured at 595 nm with a spectrophotometer plate reader. Saponin at 1 mg/mL was used as cellular death control and its absorbance was subtracted from the other values.

2.5. Neuroprotection and mitochondrial membrane potential assays

MTT assay was used to evaluate the ability of compounds to protect cells from t-butyl hydroperoxide (TBHP) damage. Cells were co-treated with complexes **1**–**4** at non-toxic concentrations (0.001, 0.01, 0.1 and 1 μM) and 75 μM TBHP for 6 h, and the assay was carried out as described above.

The mitochondrial membrane potential was assessed using the tetramethyl rhodamine methyl ester (TMRM) probe. SH-SY5Y cells were seeded in 96-well plates at a density of 5×10^4 cells per well and allowed to attach for 24 h. Cells were treated with **1**–**4** at different concentrations (0.001, 0.01, 0.1 and 1 μM) and 75 μM TBHP for 6 h. Cells were washed twice with Locke's buffer and 1 μM TMRM was added to each well for 30 min at 37 °C. After incubation, cells were solubilised with DMSO and H_2O (1:1) and the fluorescence was monitored with a spectrophotometer plate reader (535 nm excitation and 590 nm emission). The endogenous antioxidant vitamin E (Vit E) at 25 μM was used as positive control to validate the oxidative stress in vitro model.

The assay was also performed using carbonyl cyanide-*p*-trifluoromethoxyphenylhydrazone (FCCP) as $\Delta\Psi_m$ uncoupler [47–48]. In this case, cells were treated with complexes at 1 μM and FCCP at different concentrations (0.01, 0.1 and 1 μM), and TMRM assay was carried out as described above. The known mitochondrial permeability transition pore inhibitor cyclosporin A (CsA) at 2 μM was used as positive control. All experiments were performed at least three times.

2.6. Determination of ROS production

Intracellular ROS production was evaluated with the fluorescent dye carboxy-H_2DCFDA (6-carboxy-2′,7′-dichlorodihydrofluorescein diacetate) [49]. Cells were co-treated with complexes **1–4** at concentrations between 0.001 and 1 μM and 75 μM TBHP for 6 h. After this time, cells were washed with medium without serum and 20 μM carboxy-H_2DCFDA dissolved in serum-free medium was added for 1 h at 37 °C. Then, PBS was added to each well and cells were incubated for 30 min before measuring the fluorescence with a spectrophotometer plate reader (495 nm excitation and 527 nm emission). Experiments were performed at least three times by triplicate. The known antioxidant Vitamin E (Vit E) at 25 μM was used as positive control to validate the assay.

2.7. Confocal microscopy images

Human neuroblastoma cells were seeded in 12-well plates at density of 3×10^5 cells per well and allowed to grow for 24 h. Then, cells were washed twice with Locke's buffer and treated with complexes **1–4** at 1 μM for 10 min and 37 °C. Fluorescence images were obtained in a Nikon Eclipse TE2000-E inverted microscope attached to a C1 laser confocal system and EZ-C1 V.2.20 software (Nikon Instruments Europe B.V., Amstelveen, Netherlands) by using the 405 nm laser and 520 nm emission filter. The images were collected using 20× oil immersion objective (Nikon).

2.8. Statistical analysis

Data are presented as mean ± SEM (standard error of mean) of three independent replicates. Statistical differences were evaluated by Student's *t*-test with Graph Pad Prism 6 software. Statistical significance was considered at $p < 0.05$.

3. Results and discussion

3.1. Synthesis and characterization of ligands and metal complexes

H_2L^2 and H_2L^3 were successfully obtained by the synthetic route detailed in the experimental section. All the ligands were isolated with high yield and purity as confirmed by several analytical and spectroscopic techniques. All these data are available in the Supplementary Information section. Mass spectra of H_2L^2 and H_2L^3, ^{1}H NMR and ^{13}C NMR spectra for H_2L^0, H_2L^2 and H_2L^3 are collected in Figs. S1-S8.

The electrochemical methodology was used to obtain neutral compounds: Oxidation of the manganese anode in an acetonitrile solution containing the corresponding ligand and a small amount of tetraethylammonium perchlorate as supporting electrolyte gave rise to electrochemical efficiency values close to 0.5 mol F^{-1} for Mn(II) complexes. Elemental analyses establish a formula $Mn(L^n).xH_2O$, also supported by other spectroscopic techniques. The existence of peaks corresponding to the species $[ML + H]^+$ in the mass spectra of the complexes confirms the

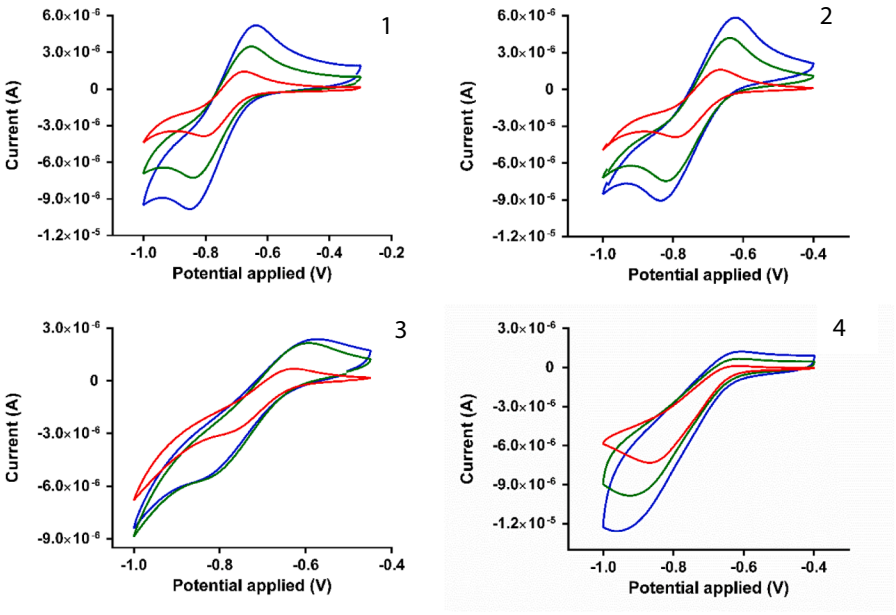

Fig. 1. Cyclic voltammograms for **1**–**4** at different scan rates: 0.02 V s^{-1} (blue), 0.05 V s^{-1} (green) and 0.09 V s^{-1} (red). (For interpretation of the references to colour in this figure legend, the reader is referred to the web version of this article.)

coordination of the different ligands to the manganese ion (Fig. S9-S10). The effective Bohr magneton numbers are very close to the spin-value of 5.9 B. M., as expected for a high-spin magnetically diluted d^5 manganese (II) ion. The anionic character of the ligands H_2L^2 and H_2L^3 were confirmed by IR spectroscopy, after the disappearance in the IR spectra of complexes **2** and **3** (Figs. S11-S12) of the NH bands from the free ligand. These changes suggest the deprotonation of the sulphonamide group in **2** [44], and the sulphonamide and thiosemicarbazide groups in **3** [42]. The IR spectra of the complexes show the shift of the ν(C=N + C-N) (and ν(C—S) in **3**) bands to lower frequencies in comparison with those of the free ligands. The hydrate nature of the complexes, suggested by elemental analyses, is confirmed by the presence of ν(OH) bands at around 3400 cm^{-1}. It must be noted that in complex **2**, the deprotonation of the phenolic -OH group located at the coordination site of $[L^2]^{2-}$ can only be confirmed with the analytical and ESI-MS data, as ν(OH) bands due to a further phenolic -OH substituent and water molecules are observed in the IR spectrum of **2**. Hence the coordination behaviour of ligand H_2L^2 is similar to that observed for the ligand H_2L^1 previously reported by us [44]. In complex **3**, the coordinated ligand is deprotonated at the suphonamide NH and the hydrazide NH group from the thiosemicarbazone moiety. The dianionic ligand $[L^3]^{2-}$ binds to the Mn (II) ion through a pentadentate $[N_4S]$ donor site that comprises a sulphonamide nitrogen atom, two imine nitrogen atoms, one pyridine nitrogen atom and a thiolate sulfur atom. Taking into account the presence of water molecules in $MnL^3.4H_2O$ (**3**), distorted pentagonal-bipyramidal coordination geometry with two water molecules occupying the axial positions could be proposed for this complex.

The Mn(II) complexes were characterized by cyclic voltammetry measurements recorded from DMSO solutions of the complexes in 0.1 M tetraethylammonium perchlorate. Fig. 1 shows the voltammograms at different scan rates. The Mn(II) complexes undergo one oxidation process to form the Mn(III) species. The redox properties of the four manganese(II) complexes showed grossly similar behaviour consisting of a quasi-reversible Mn(II)/Mn(III) oxidation, with peak to peak separation in the range 130 to 230 mV. The degree of reversibility is higher for **1** and **2**, and decreases for complexes **3** and **4**. The separation of the anodic and cathodic waves increases upon increasing the scan rate. As is predictable, the intensity of the current also increased at higher scan rates since faster scan rates lead to a decrease in the size of the diffusion layer.

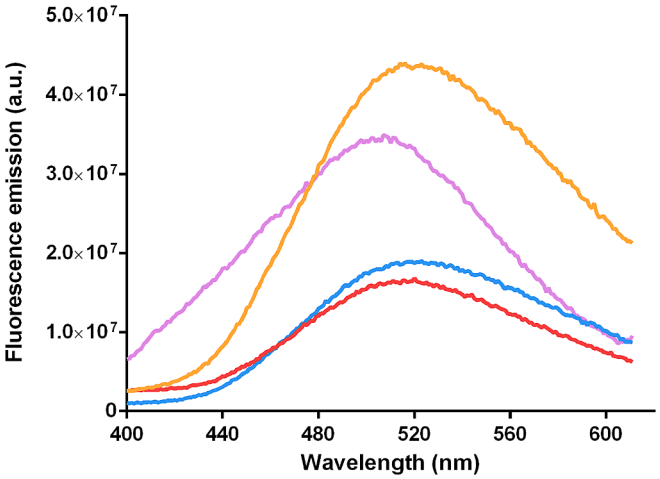

Fig. 2. Overlapped fluorescence emission spectra recorded in dimethyl sulfoxide for **1** (λ_{exc} = 325 nm, λ_{em} = 520 nm, orange spectrum), **2** (λ_{exc} = 325 nm, λ_{em} = 515 nm, red spectrum), **3** (λ_{exc} = 325 nm, λ_{em} = 520 nm, blue spectrum), and **4** (λ_{exc} = 310 nm, λ_{em} = 505 nm, purple spectrum). (For interpretation of the references to colour in this figure legend, the reader is referred to the web version of this article.)

The $E_{1/2}$ values for the Mn(II)/(Mn(III) redox couple lie in between −730 mV and

-830 mV, similar to other reported Mn(II)/Mn/(III) complexes [50–53]. At this point it may be mentioned that the redox potential of the manganese complexes is extremely sensitive to the environment surrounding the metal ion [54]. The values obtained for **1**–**4** are in the lower part of the vast window of reported redox potentials for manganese(II) complexes [55–56].

Complexes **1**–**4** show fluorescence emission characterized by a single band (Fig. 2) as result of the incorporation of the 2-tosylaminobenzaldehyde or dansyl fluorophores into the ligands. This feature allowed us to follow the distribution of these complexes in cell studies. The fluorescence emission spectra of **1**–**4** were recorded from 4×10^{-7} M solutions in dimethyl sulfoxide.

The maximum emission for **1** and **2** is shifted compared to the fluorescence emission of the free ligands (i.e. from λ_{em} at 559 nm

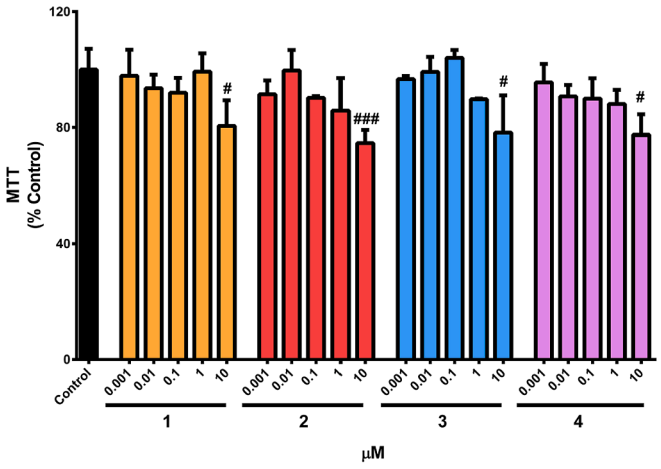

Fig. 3. Viability of cells treated with complexes **1**–**4**. SH-SY5Y cells were treated with compounds for 24 h and their cytotoxic effects were determined with MTT assay. Values are mean ± SEM of three independent replicates, expressed as percentage of untreated control cells. Statistical differences determined by Student's *t*-test. #$p < 0.05$, ###$p < 0.001$ compared to control cells.

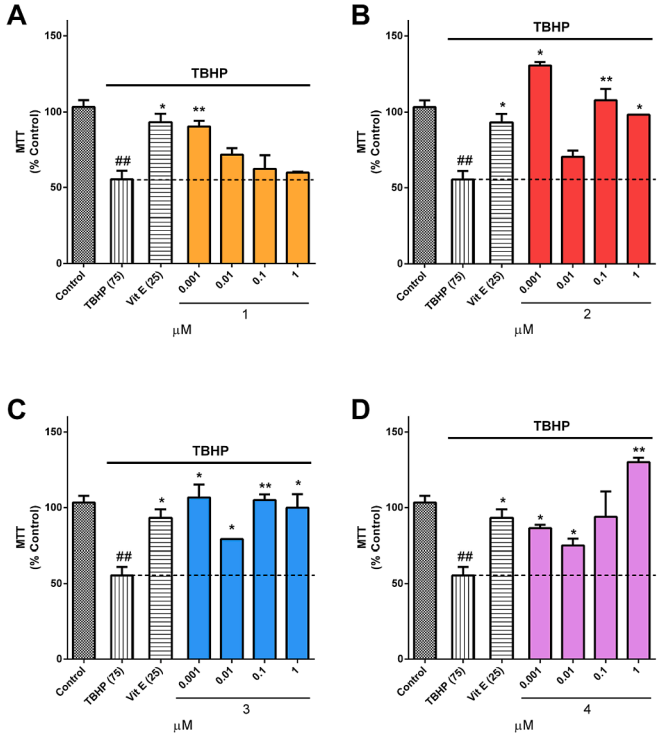

Fig. 4. Evaluation of the neuroprotective effect of compounds in an oxidative stress model. SH-SY5Y cells were co-treated with 75 μM TBHP and compounds (0.001–1 μM) for 6 h. Their effect on cell viability was assessed by MTT test and Vitamin E was used as positive control. (A) Compound **1,** (B) Compound **2**, (C) Compound **3** (D) Compound **4**. Data are mean ± SEM of three experiments performed by triplicate. Values are expressed as percentage of control cells. Statistical differences determined by Student's *t*-test. ##$p < 0.01$ compared to control cells and *$p < 0.05$, **$p < 0.01$ compared to cells treated with TBHP alone.

observed in H_2L^1 to $\lambda_{em} = 520$ nm in **1**; from λ_{em} at 535 nm in H_2L^2 to λ_{em} at 515 nm in **2**), as shown in Figs. S13-S14. In the case of complexes **3** and **4** and their ligands, there is a coincidence in the fluorescent emission bands (at ca. 510–520 nm).

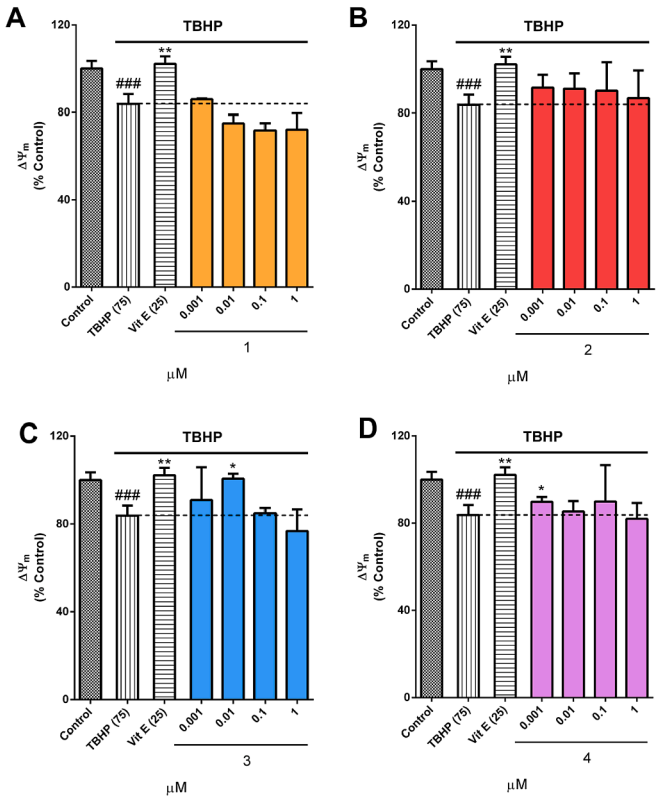

Fig. 5. Effect of complexes on $\Delta\Psi_m$ in human neuroblastoma cells. Compounds (0.001–1 μM) and 75 μM TBHP were added to the cells for 6 h. The fluorescent dye TMRM was used to evaluate their effect on $\Delta\Psi_m$. Effects of (A) complex **1**, (B) complex **2**, (C) complex **3** and (D) complex **4**. Mean ± SEM of three independent experiments. Values are expressed as percentage of control cells. Data compared to control cells (###$p < 0.001$) and cells treated with TBHP alone (*$p < 0.05$, **$p < 0.01$) by Student's *t*-test.

Stability studies over time of solutions of the four complexes have been carried out. UV–Vis studies (Fig. S15) confirm the stability of the complexes in the incubation time periods used in the biological studies.

3.2. *Protective effects of complexes 1–4 on SH-SY5Y cells*

At first, the cytotoxic effects of compounds **1–4** were assessed. Cells were treated with concentrations ranging from 0.001 to 10 μM for 24 h and MTT assay was performed. As Fig. 3 shows, all the complexes presented cytotoxic effects at the highest concentration (10 μM), so this dose was excluded in the following experiments.

Next, the antioxidant properties of compounds were determined. For these assays, TBHP was used as oxidant to induce cell damage. Cells were co-treated with **1–4** at non-toxic concentrations (0.001–1 μM) and 75 μM TBHP for 6 h [20]. In order to validate the model, Vit E at 25 μM was used as antioxidant control (Fig. 4).

Treatment with **1** produced a significant increase in cell survival at 0.001 μM (90.3 ± 3.8%) compared with TBHP control (Fig. 4A). Compounds **2, 3** and **4** also induced a significant augmentation on cell survival, with levels between 79.1 ± 0.8% and 130.9 ± 4.1% (Fig. 4B-D). The effects produced by these compounds are not dose dependent. Natural compounds such as curcumin or resveratrol have also presented this behaviour, showing antioxidant properties at low doses and producing oxidative stress at high concentrations [57–60]. Complexes could be interacting with other cellular pathways at high concentrations, or with a receptor that could be suffering a threshold effect, so it would present greater affinity at low concentrations and would be desensitized at higher doses [61].

Next, the effects of compounds **1–4** on $\Delta\Psi_m$ were determined with

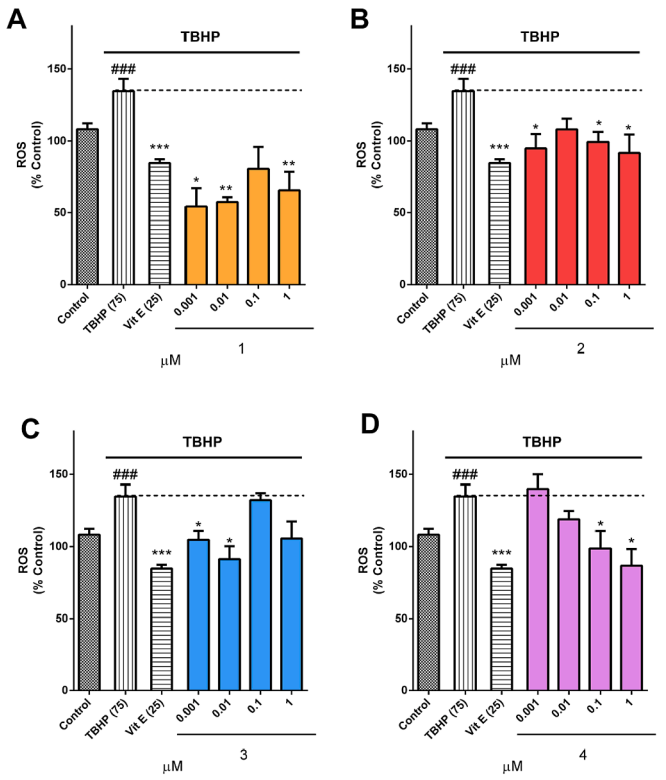

Fig. 6. Effect of **1**–**4** on ROS levels in human neuroblastoma cells. Cells were co-treated with compound **1** (A), compound **2** (B), compound **3** (C) and compound **4** (D) at concentrations ranging from 0.001 to 1 μM and 75 μM TBHP for 6 h. ROS production was evaluated with the fluorescent dye carboxy-H_2DCFDA. Vit E was used as positive control. Mean ± SEM of three independent experiments. Data are expressed as percentage of control cells. Statistical differences with respect to control cells (###$p < 0.001$) and THBP control (*$p < 0.05$, **$p < 0.01$, ***$p < 0.001$) were determined with Student's *t*-test.

TMRM dye, which accumulates in mitochondria in inverse proportion to $\Delta\Psi_m$. The potential interferences between compounds and TMRM fluorescence were assessed before performing the cellular assay. As expected, due to the differences in excitation and emission wavelengths, no variations in TMRM signal were observed in the presence of complexes (data not shown).

Therefore, cells were co-treated with compounds (0.001–1 μM) and 75 μM TBHP for 6 h. TBHP addition produced a decrease in $\Delta\Psi_m$ of 78.7 ± 2.3% compared to control cells. This diminution was reversed by treatment with 25 μM Vit E, which increased $\Delta\Psi_m$ by 102.1 ± 3.5% (Fig. 5).

Complexes **1** and **2** had no effect on the restoration of $\Delta\Psi_m$ levels when co- treated with TBHP. Compound **3** had effect at 0.01 μM, with an increase of 100.6 ± 0.1% (Fig. 5C), and complex **4** produced an augmentation on $\Delta\Psi_m$ of 89.8 ± 0.3% at the lowest concentration of study (Fig. 5D).

Then, the effect of compounds on ROS production was analysed. Before performing the assay, carboxy-H_2DCFDA fluorescence was monitored in the presence of complexes **1–4**. No interferences were detected (data do not show), so the experiment was carried out. Cells were co-treated with complexes **1–4** and TBHP as described before, and the levels of these damaging molecules were evaluated with a fluorimetric assay (Fig. 6).

Co-treatment with **1** and TBHP produced a significant decrease of ROS, with levels of 54.2 ± 9.0%, 57.3 ± 2.4% and 68.5 ± 10.6% at 0.001, 0.01 and 1 μM, respectively (Fig. 6A). Addition of compound **2** at 0.001, 0.1 and 1 μM also generated a significant decrease of ROS ($p < 0.05$) compared with TBHP control (Fig. 6B). Complex **2** was able to decrease the oxidant species about 40% of untreated control cells. When neuroblastoma was co-treated with TBHP and **3,** a significant decrease in ROS levels was found ($p < 0.05$), with percentages of 104.7 ± 5.0% at 0.001 μM and 91.3 ± 7.4% at 0.01 μM (Fig. 6C). Finally, co-treatment with 75 μM THBP and **4** resulted in a dose-dependent effect. Compound **4** was not able to reduce ROS production at low concentrations, but it produced a significant decrease in ROS release at 0.1 and 1 μM, with percentages of 98.6 ± 9.8% and 86.7 ± 9.5%, respectively (Fig. 6D).

Finally, as TBHP induces mitochondrial depolarization through the generation of exogenous ROS, the electronic transport chain uncoupler FCCP was added to produce an internal mitochondrial depolarization [62–63] and $\Delta\Psi_m$ was evaluated. For this experiment, compounds were used at a single concentration, 1 μM, which was selected based on the previous results. Cells were co-treated with compounds **1–4** at 1 μM and FCCP at three doses (0.01, 0.1, 1 μM), and TMRM assay was performed. CsA at 2 μM was used as positive control due to its ability to prevent mitochondrial permeability transition pore opening and thus, mitochondrial depolarization (Fig. 7).

When cells were treated with FCCP at 1 μM, a significant decrease in $\Delta\Psi_m$ was observed (61.7 ± 2.8%). In this case, compounds were not able to ameliorate mitochondrial potential like occurred with CsA (Fig. 7A). However, when FCCP was added at 0.1 and 0.01 μM, compound **4** significantly improved $\Delta\Psi_m$, reaching levels of 86.8 ± 6.2% and 85.8 ± 4.0%, respectively (Fig. 7B,C). These results were similar to the percentages obtained with 2 μM CsA, with values between 78.8 and 85.3%.

In view of the results obtained, and due to the physicochemical properties of the compounds, their ability to enter SH-SY5Y cells was assessed by confocal microscopy. Compounds were excited with a

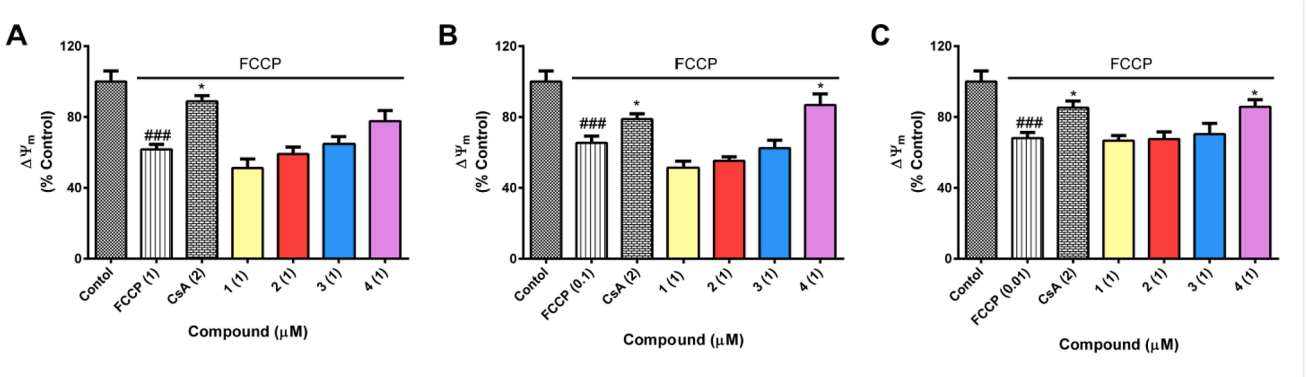

Fig. 7. Effect of **1**–**4** on mitochondrial membrane depolarization induced by FCCP in SH-SY5Y cells. Compounds at 1 μM and FCCP at 1 (**A**), 0.1 (**B**) and 0.01 μM (**C**) were added to the cells for 6 h. Mean ± SEM of three independent experiments. Data are expressed as percentage of control cells and compared to control cells (###$p < 0.01$) and to cells treated with FCCP alone (*$p < 0.05$) by Student's *t*-test.

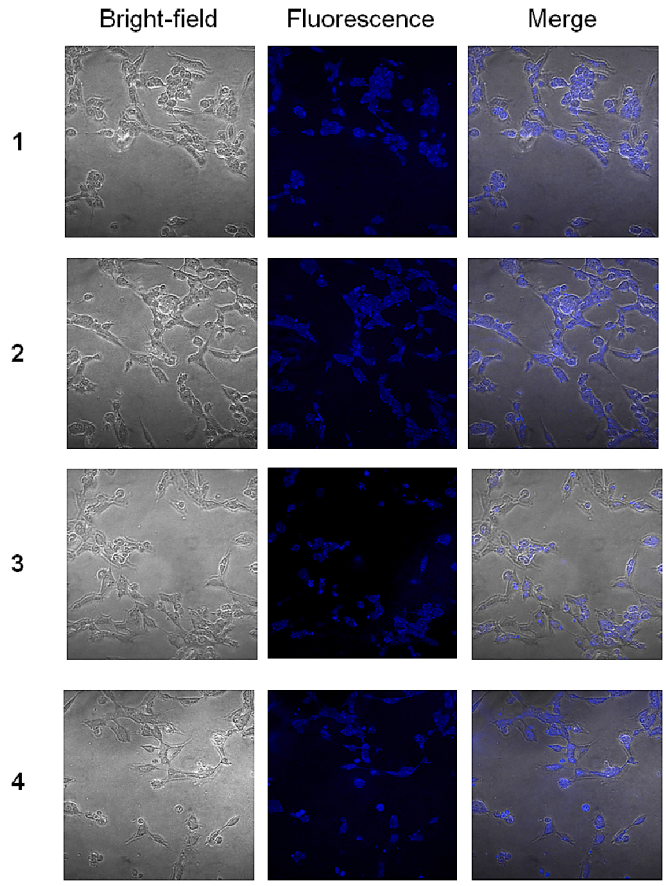

Fig. 8. Microscopy images of neuroblastoma cells treated with compounds **1–4**. SH-SY5Y cells were treated with complexes **1–4** at 1 μM for 10 min and microphotographs were obtained by confocal microscopy ($\lambda_{ex/em}$ = 405/510–525 nm).

wavelength of 405 nm and the fluorescence was recorded with a 510 nm emission filter. The microphotographs obtained confirmed the capacity of compounds to enter the cells (Fig. 8).

4. Conclusions

The incorporation of the dansyl or tosyl fluorescent dyes to four organic ligands led to four manganese(II) complexes that have been characterized using analytical and spectroscopic techniques. The complexes derived from ligands H_2L^{1-3} exhibit mononuclear stoichiometries whereas that derived from the tridentate thiosemicarbazone H_2L^4 show a dimmer structure. Fluorescent complexes **1–4** behave like biomimetic models of antioxidant enzymes, and our results indicate that manganese complexes were able to enter in neuroblastoma cells and to protect them from oxidative damage. Complexes induced a significant decrease in ROS release, being **3** and **4** the most promising ones, as these compounds were capable to restore $\Delta\Psi_m$ at low concentrations. In particular complex **4**, which recovered mitochondrial potential from FCCP and TBHP damage, could be a potential candidate for the treatment of neurodegeneration. The fluorescent properties of these complexes allow monitoring of their distribution in biological media, making them suitable for a wide variety of subsequent studies beyond their antioxidant activity.

Declaration of Competing Interest

The authors declare that they have no known competing financial interests or personal relationships that could have appeared to influence the work reported in this paper.

Acknowledgements

The research leading to these results has received funding from the following FEDER cofunded-grants. From Consellería de Cultura, Educación e Ordenación Universitaria, Xunta de Galicia, 2017 GRC GI-1682 (ED431C 2017/01), 2018 GRC GI-1584 (ED431C 2018/13), MetalBIO Network (ED431D 2017/01). From CDTI and Technological Funds, supported by Ministerio de Economía, Industria y Competitividad IIS-CIII/PI19/001248. From Ministerio de Ciencia, Innovación y Universidades, MULTIMETDRUGS (RED2018-102471-T). From European Union, Interreg AlertoxNet EAPA-317-2016, Interreg Agritox EAPA-998-2018, and H2020 778069-EMERTOX.

Appendix A. Supplementary data

Supplementary data to this article can be found online at https://doi.org/10.1016/j.jinorgbio.2021.111670.

References

[1] B. Halliwell, Nutr. Rev. 55 (1997) S44–S49.
[2] P.A. Cerutti, Eur. J. Clin. Investig. 21 (1991) 1–5.
[3] M. Seedek, G. Callera, A. Montezano, A. Gutsol, F. Heitz, C. Szyndralewiez, P. Page, C.R.J. Kennedy, K.D. Burns, R.M. Touyz, R.L. Hébert, Am. J. Physiol. Renal Physiol. 299 (2010) F1348–F1358.
[4] X.Y. Zhao, M.H. Lu, D.J. Yuan, D.E. Xu, P.P. Yao, W.L. Ji, H. Chen, W.L. Liu, C. X. Yan, Y.Y. Xia, S. Li, J. Tao, Q.-H. Ma, Front. Neurosci. 13 (2019) 30.
[5] P. Sharma, P. Srivastava, A. Seth, P.N. Tripathi, A.G. Banerjee, S.K. Shrivastava, Prog. Neurobiol. 174 (2019) 53–89.
[6] S.K. Jain, R. Parsanathan, S.N. Levine, J.A. Bocchini, M.F. Holik, J.A. Vanchiere, Free Rad. Biol. Med. 161 (2020) 84–91.
[7] A.V.W. Nunn, G.W. Guy, W. Brysch, S.W. Botchway, W. Frasch, E.J. Calabrese, J. D. Bell, Immun. Ageing 17 (2020) 33.
[8] S. Suhail, J. Zajac, C. Fossum, H. Lowater, C. McCracken, N. Severson, B. Laatsch, A. Narkiewicz-Jodko, B. Johnson, J. Liebau, S. Bhattacharyya, S. Hati, Protein J. 39 (2020) 644–656.
[9] V. Guloyan, B. Oganesian, N. Baghdasaryan, C. Yeh, M. Singh, F. Guilford, Y.-S. Ting, V. Venketaramn, Antioxidants 9 (2020) 914.
[10] R. Zhang, X. Wang, L. Ni, X. Di, B. Ma, S. Niu, C. Liu, R.J. Reiter, Life Sci. 250 (2020), 117583.
[11] A.H. Sawalha, M. Zhao, P. Coit, Q. Lu, Clin. Immunol. 215 (2020), 108410.
[12] G. Cerullo, M. Negro, M. Parimbelli, M. Pecoraro, S. Perna, G. Liguori, M. Rondanelli, H. Cena, G. D'Antona, Front. Immunol. 11 (2020), 574029.
[13] M. Zarbafian, S. Dayan, S.G. Fabi, J. Cosmet. Dermatol. 19 (2020) 3171–3176.
[14] B.B. Bakadia, B.O.O. Boni, A.A.Q. Ahmed, G. Yang, Life Sci. 264 (2021), 118653.
[15] F.A. Villamena, Mol. Basis Oxidative (2013) 1–48.
[16] L. He, T. He, S. Farrar, L.B. Ji, T.Y. Liu, X. Ma, Cell Physiol. Biochem. 44 (2017) 532–553.
[17] P. Davall, T. Mitic, A. Caporali, A. Lauriola, D. D'Arca, ROS, cell senescence, and novel molecular mechanisms in aging and age-related diseases. Oxidative Med. Cell. Longev. 46 (2016) 3565127.
[18] L. Rouco, M. Maneiro, Neural Regen. Res. 16 (2021) 121–122.
[19] E. Miller, L. Markiewicz, J. Kabzinski, D. Odrobina, I. Majsterek, Front. Biosci. 9 (2017) 214–234.
[20] L. Rouco, A. Liberato, M.J. Fernández-Trujillo, A. Máñez, M.G. Basallote, R. Alvariño, A. Alfonso, L.M. Botana, M. Maneiro, J. Inorg. Biochem. 203 (203) (2020), 110918.
[21] S.L. Huang, H.B. He, K. Zou, C.H. Bai, Y.H. Xue, J.Z. Wang, J.F. Chen, J. Pharm. Pharmacol. 66 (2014) 844–854.
[22] R. Alvariño, E. Alonso, M.A. Tribalat, S. Gegunde, O.P. Thomas, L.M. Botana, Neurotox. Res. 32 (2017) 368–380.
[23] M.A. Vázquez-Fernández, M.R. Bermejo, M.I. Fernández-García, G. González-Riopedre, M.J. Rodríguez-Doutón, M. Maneiro, J. Inorg. Biochem. 105 (2011) 1538–1547.
[24] G.N. Ledesma, E. Anxolabéhère-Mallart, L. Sabater, C. Hureau, S.R. Signorella, J. Inorg. Biochem. 186 (2018) 10–16.
[25] S. Signorella, C. Palopoli, G. Ledesma, Coord. Chem. Rev. 305 (2018) 75–102.
[26] A. Erxleben, Inorg. Chim. Acta 472 (2018) 40–57.
[27] J.C. Pessoa, I. Correia, Coord. Chem. Rev. 388 (2019) 227–247.
[28] S.R. Doctrow, K. Huffman, C. Bucay Marcus, G. Tocco, E. Malfroy, C.A. Adinolfi, H. Kruk, K. Baker, N. Lazarowych, J. Mascarenhas, B. Malfroy, J. Med. Chem. 45 (2002) 4549–4558.
[29] F.C. Friedel, D. Lieb, I. Ivanovic-Burmazovic, J. Inorg. Biochem. 109 (2012) 26–32.
[30] E. Mathieu, A.-S. Bernard, N. Delsuc, E. Quévrain, G. Gazzah, B. Lai, F. Chain, P. Langella, M. Bachelet, J. Masliah, P. Seksik, C. Policar, Inorg. Chem. 56 (2017) 2545–2555.
[31] L. Rouco, A.M. González-Noya, R. Pedrido, M. Maneiro, Antioxidants 9 (2020) 727.

[32] S. Melov, S.R. Doctrow, J.A. Schneider, J. Haberson, M. Patel, P.E. Coskun, K. Huffman, D.C. Wallace, B. Malfroy, J. Neurosci. 21 (2001) 8348–8353.
[33] T. Watanabe, S. Owada, H.P. Kobayashi, H. Kawakami, S. Nagaoka, E. Murakami, N. Tobe, A. Ishiuchi, T. Enomoto, Y. Jinnouchi, J. Sakurai, N. Tobe, S. Koizumi, T. Shimamura, T. Asakura, H. Nakano, T. Otsubo, Transplant. Proc. 39 (2007) 3002–3006.
[34] S. Melov, N. Wolf, D. Strozyk, S.R. Doctrow, A.I. Bush, Free Radic. Biol. Med. 38 (2005) 258–261.
[35] A. Clausen, S. Doctrow, M. Baudry, Neurobiol. Aging 31 (2010) 425–433.
[36] M.W. Brazier, S.R. Doctrow, C.L. Masters, S.J. Collins, Free Radic. Biol. Med. 45 (2008) 184–192.
[37] S.E. Browne, L.J. Roberts II, P.A. Dennery, S.R. Doctrow, M.F. Beal, C. Barlow, R. L. Levine, Free Radic. Biol. Med. 36 (2004) 938–942.
[38] C. Jung, Y. Rong, S. Doctrow, M. Baudry, B. Malfroy, Z. Xu, Neurosci. Lett. 304 (2001) 157–160.
[39] M.A. Miller, R. Weissleder, R. Adv, Drug Deliv. Rev. 113 (2017) 61–86.
[40] Y.-H. Li, L.-M. Chan, L. Tyer, R.T. Moody, C.M. Himel, D.M. Hercules, J. Am. Chem. Soc. 97 (1975) 3118–3126.
[41] B. Branchi, P. Ceroni, G. Bergamini, V. Balzani, M. Maestri, J. Van Heyst, S.-K. Lee, F. Luppertz, F. Vögtle, Chem. Eur. J. 12 (2006) 8926–8934.
[42] R. Pedrido, M.J. Romero, M.R. Bermejo, A.M. González-Noya, I. García-Lema, G. Zaragoza, Chem. Eur. J. 14 (2008) 500–512.
[43] M.J. Romero, R. Pedrido, A.M. González-Noya, M. Martínez-Calvo, G. Zaragoza, M. R. Bermejo, Chem. Commun. 46 (2010) 5115–5117.
[44] M.J. Romero, R. Pedrido, A.M. González-Noya, M. Maneiro, M.I. Fernández-García, G. Zaragoza, M.R. Bermejo, Dalton Trans. 41 (2012) 10832–10844.
[45] M. McCord, I. Fridovich, J. Biol. Chem. 244 (1969) 6049–6055.
[46] E. Vega-Avila, M.K. Pugsley, Proc. West. Pharmacol. Soc. 54 (2011) 10–14.
[47] G. Dispersyn, R. Nuydens, R. Connors, M. Borgers, H. Geerts, Biochimica et Biophysica Acta (BBA)-General Subjects 1428 (1999) 357–371.
[48] M. Leirós, J.A. Sánchez, E. Alonso, M.E. Rateb, W.E. Houssen, R. Ebel, M. Jaspars, A. Alfonso, L.M. Botana, Marine drugs 12 (2014) 700–718.
[49] L.M. Tetz, P.W. Kamau, A.A. Cheng, J.D. Meeker, R. Loch-Caruso, J. Pharmacol. Toxicol. Methods 67 (2013) 56–60.
[50] R. Hage, B. Krijnen, J.B. Warnaar, F. Hartl, D.J. Stufkens, T.L. Snoeck, Inorg. Chem. 34 (1995) 4973–4978.
[51] S. Abdolahzadeh, J.W. de Boer, W.R. Browne, Eur. J. Inorg. Chem. (2015) 3432–3456.
[52] M.B. Solomon, B. Chan, C.P. Kubiak, K.A. Jolliffe, D.M. D'Alessandro, Dalton Trans. 48 (2019) 3704–3713.
[53] M. Enamullah, M.A. Zaman, M.M. Bindu, D. Woschko, M.K. Islam, C. Janiak, J. Mol. Struct. 1239 (2021), 130455.
[54] M. Sjödin, J. Gätjens, L.C. Tabares, P. Thuéry, V.L. Pecoraro, S. Un, Inorg. Chem. 47 (2008) 2897–2908.
[55] S. Komorsky-Lovric, J. Electroanal. Chem. 397 (1995) 211–215.
[56] C. Palopoli, J. Ferreyra, A. Conte-Daban, M. Richezzi, A. Foi, F. Doctorovich, E. Anxolabéhère-Mallart, C. Hureau, S.R. Signorella, ACS Omega 4 (2019) 48–57.
[57] N.S.A. Moghaddam, M.N. Oskouie, A.E. Butler, P.X. Petit, G.E. Barreto, A. Sahebkar, J. Cell. Physiol. 234 (2019) 10060–10071.
[58] A.M. Posadino, A. Cossu, R. Giordo, A. Zinellu, S. Sotgia, A. Vardeu, G. Pintus, Food Chem. Toxicol. 78 (2015) 10–16.
[59] Y. Hirata, K. Kuwabara, M. Takashima, T. Murai, Chem. Res. Toxicol. 33 (2020) 2892–2902.
[60] E.J. Calabrese, W.J. Kozumbo, Pharmacol. Res. 163 (2021), 105283.
[61] R.J. Williams, J.P. Spencer, Free Radic. Biol. Med. 52 (2012) 35–45.
[62] J.A. Sánchez, A. Alfonso, M. Leirós, E. Alonso, M.E. Rateb, M. Jaspars, W. E. Houssen, R. Ebel, L.M. Botana, Cell. Physiol. Biochem. 37 (2015) 779–792.
[63] K.S. Park, I. Jo, Y. Pak, S.-W. Bae, H. Rhim, S.-H. Suh, S. Park, M. Zhu, I. So, K. Kim, Pflügers Arch - Eur J Physiol 443 (2002) 344–352.